university of groningen

University Medical Center Groningen

University of Groningen

# A fast electrochemical actuator in the non-explosive regime

Uvarov, Ilia V.; Melenev, Artem E.; Lokhanin, Mikhail V.; Naumov, Victor V.; Svetovoy, Vitaly B.

*Published in:*
Journal of Micromechanics and Microengineering

*DOI:*
10.1088/1361-6439/ab3bde

**IMPORTANT NOTE: You are advised to consult the publisher's version (publisher's PDF) if you wish to cite from it. Please check the document version below.**

*Document Version*
Publisher's PDF, also known as Version of record

*Publication date:*
2019

Link to publication in University of Groningen/UMCG research database

*Citation for published version (APA):*
Uvarov, I. V., Melenev, A. E., Lokhanin, M. V., Naumov, V. V., & Svetovoy, V. B. (2019). A fast electrochemical actuator in the non-explosive regime. *Journal of Micromechanics and Microengineering*, *29*(11), [114001]. https://doi.org/10.1088/1361-6439/ab3bde

**Copyright**
Other than for strictly personal use, it is not permitted to download or to forward/distribute the text or part of it without the consent of the author(s) and/or copyright holder(s), unless the work is under an open content license (like Creative Commons).

The publication may also be distributed here under the terms of Article 25fa of the Dutch Copyright Act, indicated by the "Taverne" license. More information can be found on the University of Groningen website: https://www.rug.nl/library/open-access/self-archiving-pure/taverne-amendment.

**Take-down policy**
If you believe that this document breaches copyright please contact us providing details, and we will remove access to the work immediately and investigate your claim.

*Downloaded from the University of Groningen/UMCG research database (Pure): http://www.rug.nl/research/portal. For technical reasons the number of authors shown on this cover page is limited to 10 maximum.*

Download date: 12-10-2022

Journal of Micromechanics and Microengineering

PAPER

# A fast electrochemical actuator in the non-explosive regime

To cite this article: Ilia V Uvarov *et al* 2019 *J. Micromech. Microeng.* **29** 114001

View the article online for updates and enhancements.

You may also like

- Gelatin methacryloyl is a slow degrading material allowing vascularization and long-term use *in vivo*
Stefanie Heltmann-Meyer, Dominik Steiner, Claudia Müller et al.
- A New Equation of State for Dense Hydrogen–Helium Mixtures. II. Taking into Account Hydrogen–Helium Interactions
Gilles Chabrier and Florian Debras
- Energy efficiency of production of Vico-oat mixture at various cultivation technologies
T P Sabirova, G S Galina and P Sabirov


ECS Membership = Connection

ECS membership connects you to the electrochemical community:

- Facilitate your research and discovery through ECS meetings which convene scientists from around the world;
- Access professional support through your lifetime career:
- Open up mentorship opportunities across the stages of your career;
- Build relationships that nurture partnership, teamwork—and success!

Join ECS! Visit electrochem.org/join

This content was downloaded from IP address 129.125.19.61 on 29/07/2022 at 15:07

IOP Publishing Journal of Micromechanics and Microengineering
J. Micromech. Microeng. **29** (2019) 114001 (8pp) https://doi.org/10.1088/1361-6439/ab3bde

# A fast electrochemical actuator in the non-explosive regime

**Ilia V Uvarov[1], Artem E Melenev[1], Mikhail V Lokhanin[2], Victor V Naumov[1] and Vitaly B Svetovoy[3,4]**

[1] Valiev Institute of Physics and Technology of Russian Academy of Sciences, Yaroslavl Branch, Universitetskaya 21, 150007 Yaroslavl, Russia
[2] P.G. Demidov Yaroslavl State University, Sovetskaya 14, 150003 Yaroslavl, Russia
[3] Zernike Institute for Advanced Materials, University of Groningen, Nijenborgh 4, 9747 AG Groningen, The Netherlands
[4] A.N. Frumkin Institute of Physical Chemistry and Electrochemistry RAS, Leninsky pr. 31, 199071 Moscow, Russia

E-mail: i.v.uvarov@bk.ru

Received 6 May 2019, revised 8 August 2019
Accepted for publication 16 August 2019
Published 2 September 2019

**Abstract**

Microfluidic systems require a compact, energy-efficient and microtechnology-compatible actuator that pushes the liquid through the channels. Electrochemical devices are promising candidates, but they suffer from a long response time due to slow gas recombination. An actuator with a millisecond response time was demonstrated recently. A micron-sized chamber of the device with two titanium electrodes is sealed by a polydimethylsiloxane membrane. A series of microsecond voltage pulses of alternating polarity is applied to the electrodes. Nanobubbles generated in the chamber push the membrane up, but disappear quickly due to spontaneous combustion of hydrogen and oxygen. In this work, operation of the device is investigated in detail. The pulses with a frequency from 100 to 500 kHz are used for actuation. It is demonstrated that higher frequency and higher amplitude of the pulses provide larger deflection of the membrane, but finally the deflection is saturated. The stroke of 8–9 $\mu$m can be achieved. In a cyclic operation regime the actuator is driven by series of pulses. If the time interval between the series is too short, the gas accumulates in the chamber. The membrane lifts during several cycles and then oscillates in the lifted position. In this regime the operating frequency as high as several hundred hertz can be achieved. The higher the frequency, the higher is the lift. The stroke also increases with the frequency, making a higher value more beneficial. Destruction of the electrodes is not observed, but the oxidation of titanium with time suppresses the gas production and decreases the membrane deflection. At a high frequency of the pulses the oxidation goes slower, but still significantly affects the performance. The oxidation of the electrodes is recognized as the main problem of the device. Methods to solve the problem are proposed.

Keywords: electrochemical actuators, water electrolysis, nanobubbles, microfluidics

(Some figures may appear in colour only in the online journal)

## 1. Introduction

Microfluidic systems are widely used in biological and medical applications [1, 2]. A key element of the microfluidic devices, such as laboratories on a chip [3, 4] or portable and implantable drug delivery systems [5, 6], is a pump that creates a liquid flow. Typically, the pump consists of a chamber, which is filled with a working fluid and covered by a movable membrane, and two check valves [7]. The membrane moves back and forth, and pumps the fluid through the chamber in the direction determined by the valves. Performance of the pump mainly depends on the mechanism driving the membrane.

 © 2019 IOP Publishing Ltd Printed in the UK

Several actuation principles are implemented, such as piezoelectric [8, 9], electrostatic [10, 11], electromagnetic [12], thermal [13, 14] and other. Piezoelectric actuators have short response time and a large actuation force, but they are limited by a large size, high driving voltage and poor compatibility with standard microfabrication technology. Electrostatic devices are also fast, but they provide rather weak forces. Electromagnetic and thermal actuation requires a low operating voltage. However, these actuators consume significant power and generate heat. Thus, there is an acute shortage of simple, compact and energy-efficient actuators, which can be easily integrated into microfluidic systems.

Another popular method to drive membrane motion is the electrochemical actuation [15–26]. A main part of the electrochemical actuator is a working chamber filled with an aqueous electrolyte solution and covered by a flexible membrane. The chamber contains two electrodes: one is grounded (cathode), and the other one (anode) is kept at a constant current or voltage. During electrochemical decomposition of water, $H_2$ and $O_2$ bubbles emerge at the cathode and the anode, respectively. These bubbles create an overpressure that pushes the membrane. After switching the voltage off the gases recombine back into water and the membrane returns to the initial state. Electrochemical principle has a number of advantages in comparison with other actuation methods. It provides large driving force and stroke, low heat generation and power consumption, allows simple design of the actuator that is easy to fabricate and integrate with other microfluidic parts. However, conventional actuators based on DC electrolysis have very long response time due to the slow gas recombination. In order to accelerate the reverse reaction between hydrogen and oxygen, the electrodes are fabricated from platinum that demonstrates catalytic properties [15–21]. Additional means such as Nafion coating of the electrodes [16–18], platinum mesh in the working chamber [19, 20], platinum wires floating in the electrolyte [21], or platinum black [22, 23], intensify the recombination. However, the disappearance of bubbles still takes several minutes. Cyclic operation of such actuators can be performed at a quite low frequency of about 0.01 Hz.

Response time of the electrochemical actuators can be significantly reduced using the alternating polarity (AP) electrolysis instead of the usual DC process. When a series of microsecond voltage pulses of AP is applied to the working electrode while the other one is grounded, both $H_2$ and $O_2$ gases are produced above each electrode. Switching the voltage polarity at a frequency of ~100 kHz limits the size of the gas bubbles by the value of about 100 nm [27]. The pressure in the chamber increases and pushes the membrane up. When the pulses are switched off, the nanobubbles of $H_2$ and $O_2$ merge and the mixture of gases turns back into water in milliseconds. Such a fast termination of gas is possible due to combustion of hydrogen and oxygen in nanobubbles [28]. A series of the combustion reactions occurs spontaneously at room temperature that cannot be explained in the standard combustion theory. The mechanism of this combustion is associated with a high surface-to-volume ratio (~$10^7$ $m^{-1}$) for nanobubbles. It was suggested [29] that radicals needed to ignite the reaction are generated on charged sites at the gas–liquid interface (bubble walls). In this case the reactions can proceed spontaneously at room temperature as was demonstrated by solving the kinetic equations directly [30] or using the molecular dynamics simulations [31].

An actuator based on the AP electrolysis was demonstrated recently. A working chamber with two titanium electrodes inside had a diameter of 500 $\mu$m and a height of 8 $\mu$m. It was sealed by a polydimethylsiloxane (PDMS) membrane of 30 $\mu$m thick. Design of the device and the fabrication procedure were described in the paper [32]. Our subsequent study [33] was devoted to the testing of the actuator. The electrochemical process was driven by the AP pulses with a frequency of 500 Hz. Two operation regimes of the device were demonstrated. In the first one, a series of pulses applied to the electrodes fills the chamber with nanobubbles, which are terminated quickly when the voltage is turned off. The actuator operated at the frequencies as high as 667 Hz that is five orders of magnitude faster than the conventional DC actuators. The other regime is realized at higher amplitude of the pulses. When the concentration of nanobubbles in the chamber reaches a critical value, they merge into a microbubble that explodes with the release of a large amount of energy. This regime provides up to 10 times higher stroke in comparison with the non-explosive operation. However, a special technique is required to prevent the growth of pinned bubbles during the periodic explosions.

This work describes operation of the fast electrochemical actuator in the non-explosive regime in some detail. The frequency of driving pulses varies from 100 to 500 kHz, and the dependence of the membrane deflection on this frequency is investigated. We test the device in the cyclic operation and show how the steady state regime is reached, i.e. how the stroke and position of the membrane change from cycle to cycle, and how these parameters depend on the operating frequency. The long-term stability and power consumption of the device are also analyzed. This information is necessary for choosing optimal operation conditions of the actuator and for development of a micropump based on this device.

## 2. Methods

The actuator ready for the test is shown in figure 1. A working chamber of 500 $\mu$m in diameter is located at the center of the chip. The bottom wall of the chamber is an oxidized silicon wafer with two planar electrodes of a concentric shape. The electrodes are fabricated by magnetron sputtering and consist of a 0.5 $\mu$m thick aluminum layer covered by a 0.5 $\mu$m thick titanium layer. The side walls are made of cured SU-8 resist. The chamber is sealed by a 30 $\mu$m thick PDMS membrane that is fabricated on a separate wafer and transferred to the chip using a thick PDMS structure. Bonding of PDMS to SU-8 is performed by the treatment of PDMS in nitrogen plasma. We use the same design of the actuator that was presented in our previous work [33]. The only change is the height of the chamber, which is increased from 8 to 16 $\mu$m in order to prevent stiction of the membrane to the bottom wall during the bonding.

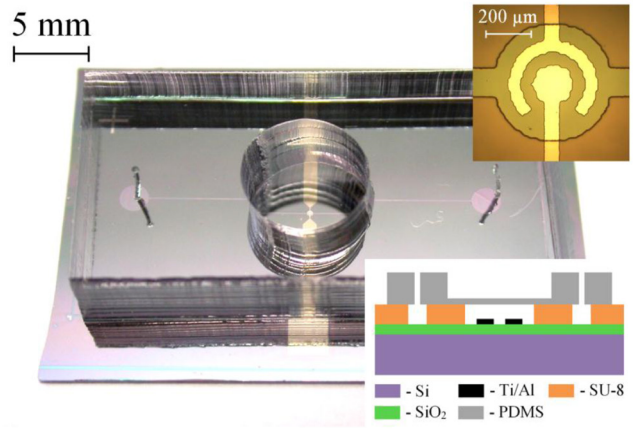


**Figure 1.** A photo of the actuator. The insets show a close-up view of the working chamber and a schematic cross-section of the device.

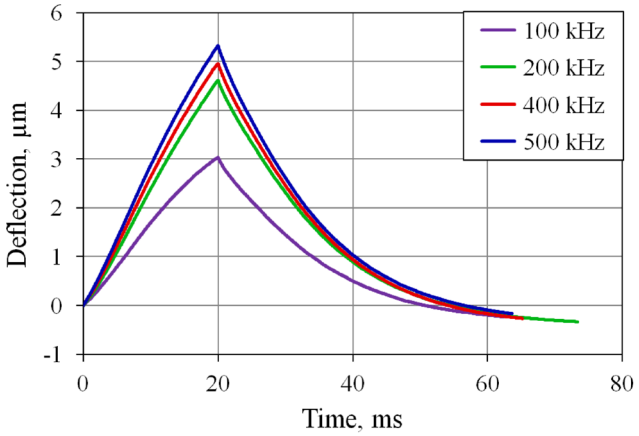


**Figure 2.** Deflection of the membrane as a function of time. Voltage pulses of the AP are applied to the electrodes during the first 20 ms. The amplitude of pulses is $U = 13$ V and the frequency $f$ varies from 100 to 500 kHz.

The working chamber is filled with an electrolyte (a molar solution of $Na_2SO_4$ in distilled water) via the holes punched in the thick PDMS structure. The holes are closed by a tape after the filling. Electrochemical process is performed by a series of rectangular voltage pulses of a positive and negative polarity applied to the working electrode while the other electrode is grounded. The voltage is provided by a homemade PC-controlled signal generator based on the microcontroller STM32F051R8T6. The signal produced by the microcontroller using direct digital synthesis method is amplified 20 times by a built-in class AB power amplifier. The maximal achievable frequency of the pulses is 500 kHz and the maximal amplitude is ±22 V. The voltage and current flowing through the electrodes are recorded by a Pico Scope 5000. Deflection of the membrane with time is measured using a homemade homodyne Michelson interferometer, which provides two phase-shifted output signals [33]. A laser beam is focused on the center of the membrane during the measurement. The membrane is covered by a 20 nm thick Al layer in order to obtain reflectivity. The signals are also captured by the oscilloscope with the sampling rate of about $3 \times 10^7$ MS $s^{-1}$, so each signal contains several millions points. Before extraction of the membrane deflection, the signals are downsampled in order to get rid of noise and to reduce the calculation time. As a result, deflection curve typically contains several thousand points. Degradation of the electrodes is investigated for the samples with the transparent membrane.

## 3. Results and discussion

### *3.1. Actuation by the pulses of various frequencies*

To achieve a better performance of the actuator, it is necessary to choose the frequency $f$ of the AP pulses that provides the largest deflection of the membrane. Figure 2 shows the time dependence of the deflection when a single series of pulses is applied to the electrodes. Four values of the frequency are used: 100, 200, 400 and 500 kHz. The number of pulses $N$ is chosen in such a way that the duration of the series (the active time) is $t_a = N/2f = 20$ ms. For $f = 100$ kHz this number is 4000, while for $f = 500$ kHz the series consists of $N = 20\,000$ pulses. The amplitude of pulses $U$ is 13 V in all cases. The membrane moves upwards during the active time. The higher the frequency, the larger is the maximal deflection $d_{max}$ (stroke). At $f = 100$ kHz the membrane rises up to $d_{max} = 3.0$ $\mu$m, while at $f = 500$ kHz the maximal deflection is $d_{max} = 5.3$ $\mu$m. The increase in the frequency from 100 to 200 kHz gives the largest increment of 1.6 $\mu$m to $d_{max}$. The further increase in the frequency increases the stroke by only 0.7 $\mu$m. After switching the pulses off, the membrane returns to the lowest position in 40–60 ms. This relaxation time is determined by the gas recombination rate and the elastic properties of the membrane.

The dependence of the stroke on the amplitude of pulses is shown in figure 3. The membrane deflection increases with $U$ for all the values of $f$. The higher the frequency $f$, the larger is the stroke. Frequencies of 400 and 500 kHz provide close values. The difference between these frequencies is perceptible only at $U = 12$–14 V. During the measurement, the amplitude of pulses can be increased only up to a threshold voltage $U_{th}$, at which the explosion of a microbubble occurs in the chamber. The threshold voltage is about 14.5 V for the frequencies of 400 and 500 kHz. The stroke of 8–9 $\mu$m can be achieved in these cases. For $f = 100$ and 200 kHz the explosions happen at a slightly lower amplitude $U_{th} \approx 13.5$ V. This is probably due to a larger size of nanobubbles generated at these frequencies [27]. The highest stroke that can be achieved at $f = 200$ kHz is about 5 $\mu$m, while at $f = 100$ kHz one can reach $d_{max} = 3$ $\mu$m. It is worth noting that the obtained values of $U_{th}$ are valid only for the selected $t_a = 20$ ms. The threshold voltage is higher for the shorter series [33], since the higher amplitude of pulses is needed to reach the critical concentration of nanobubbles during the shorter active time.

Deflection of the membrane at $f = 500$ kHz is consistent with our previous results. For a 20 ms long series, the amplitude of 10.0–13.4 V provided the stroke of 2.3–8.3 $\mu$m [33], while in the present study the membrane deflects at 1.3–8.9 $\mu$m when $U = 9$–14 V is applied (figure 3).

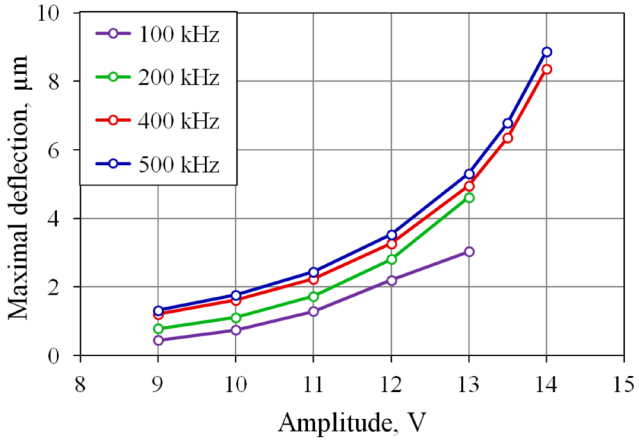


**Figure 3.** Dependence of the stroke on the amplitude of pulses for different frequencies. The amplitude is restricted by the threshold voltage. The actuator is driven by a single series of pulses $t_a = 20$ ms long.

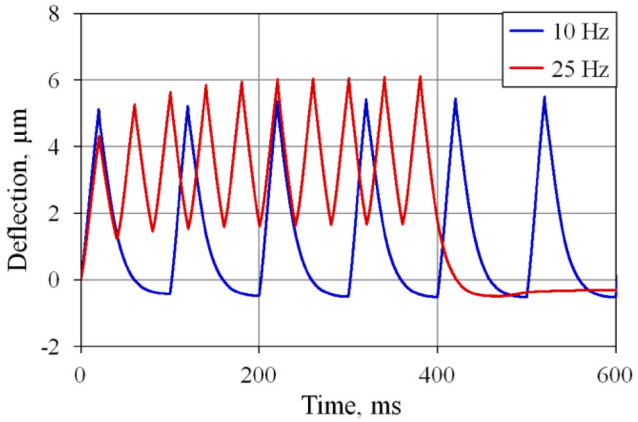


**Figure 4.** Cyclic operation of the actuator at $f_c = 10$ and 25 Hz. The process is driven by a series of $N = 20\,000$ pulses with $f = 500$ kHz and $U = 13$ V. At $f_c = 25$ Hz only ten series are applied to the sample.

### 3.2. Cyclic operation at a low operating frequency

Cyclic operation of the actuator is realized when series of pulses are repeated with the operating frequency $f_c$. The device is driven by a series of $N = 20\,000$ pulses with the frequency $f = 500$ kHz and the amplitude $U = 13$ V. The active time is $t_a = 20$ ms in this case. At these parameters the relaxation time of the membrane is 40–60 ms as can be seen in figure 2. One has to take this time into account when choosing the time interval between the series (passive time $t_p$). If $t_p = 80$ ms, the operating frequency is $f_c = 1/(t_a + t_p) = 10$ Hz. The membrane deflection at this frequency is shown by a blue line in figure 4. The membrane has enough time to return to the lowest position when the pulses are switched off. In the first cycle the stroke is $d_{max} = 5.1$ $\mu$m. It increases during the first few cycles as the chamber is saturated with nanobubbles, and then it stabilizes at $d_{max} = 6.1$ $\mu$m. At each cycle, the volume of the chamber is increased on $\Delta V = \pi r^2 d_{max}/2 = 0.6$ nl, where $r = 250$ $\mu$m is the chamber radius. An ideal pump (a pump with 100%-efficiency) based on this actuator would pump a liquid with an effective flow rate of $R = f_c \Delta V = 0.36$ $\mu$l min$^{-1}$.

One can see that after the first actuation the membrane goes below its zero position (figure 4, blue line). The same phenomenon is observed when a single series of pulses is applied to the electrodes, see figure 2. Before each test some overpressure is created in the chamber by a syringe, so that the membrane is deflected without applying voltage. This deflection is taken as a zero level. During the first few actuation cycles this pressure is partially released, which gives negative values of the deflection. After several cycles the bottom position of the membrane stabilizes at about $-0.5$ $\mu$m.

The membrane moves downwards with variable speed. The deflection is reduced by a half in the first 10 ms of the passive time, but then the movement is slowed down (figures 2 and 4). This can be explained as follows. When the membrane is in the upper position, the concentration of nanobubbles is high. The hydrogen and oxygen nanobubbles are densely packed, which facilitates the gas recombination. Due to recombination the concentration of nanobubbles is reduced and the recombination process becomes slower. It is preferable to exclude this slow movement in order to increase the operating frequency. This can be done by reducing the passive time. Operation at $f_c = 25$ Hz is shown by the red line in figure 4. A series of pulses with the same parameters as in the case of $f_c = 10$ Hz is applied to the electrodes, but $t_p$ is reduced to 20 ms. The first cycle moves the membrane nearly as high as at $f_c = 10$ Hz. The stroke is somewhat smaller (4.3 $\mu$m versus 5.1 $\mu$m), since the electrodes were oxidized during previous operation. The next series is applied before the membrane returns to the lowest position. Not all gas is terminated, and the new cycle starts from a nonzero deflection of the membrane. The starting position of the membrane gradually rises and stabilizes at 1.7 $\mu$m during the first 5–7 cycles. In the stable regime the stroke (the amplitude of oscillation) reaches the value $d_{max} = 4.5$ $\mu$m. This value is lower than the stroke at $f_c = 10$ Hz, but the effective flow rate $R = 0.66$ $\mu$l min$^{-1}$ is higher due to higher $f_c$. When the driving pulses are switched off, the membrane returns to its 'true' lowest position.

It is worth noting that the increase of the operating frequency by the reduction of the passive time has a limitation. If $t_p$ is too short, the concentration of nanobubbles may reach a critical value and an explosion may happen even at $U < U_{th}$. During the explosion a bubble grows in the chamber that isolates the electrodes from the electrolyte and normal cyclic operation fails. For the series of pulses used above, the regular operation of the device in the non-explosive mode is well achievable at $t_p \geqslant t_a$.

### 3.3. Cyclic operation at a high operating frequency

The operating frequency can be increased further by shortening the active time. Figure 5 shows the membrane deflection when a series with $t_a = 2$ ms is applied to the electrodes. A shorter series provides a lower stroke. At the amplitude $U = 13$ V that has been used previously the membrane deflects less than 0.3 $\mu$m. It is necessary to increase $U$ in order to obtain a larger stroke. At $U = 17$ V the deflection reaches 0.8 $\mu$m. For the chosen active time the threshold voltage is about 18 V. One

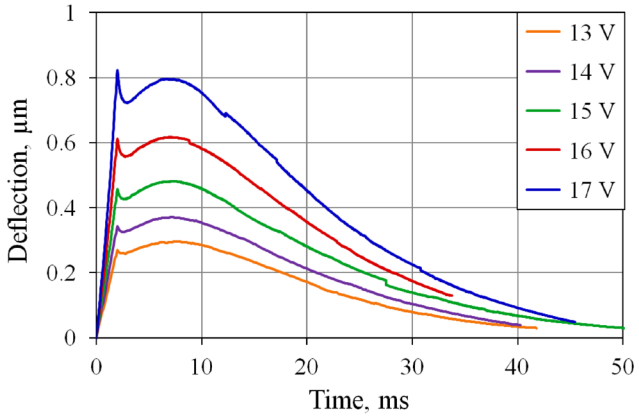


**Figure 5.** Time dependence of the membrane deflection for a single series of $N = 2000$ pulses with $f = 500$ kHz applied to the electrodes. The amplitude of the pulses varies from 13 to 17 V.

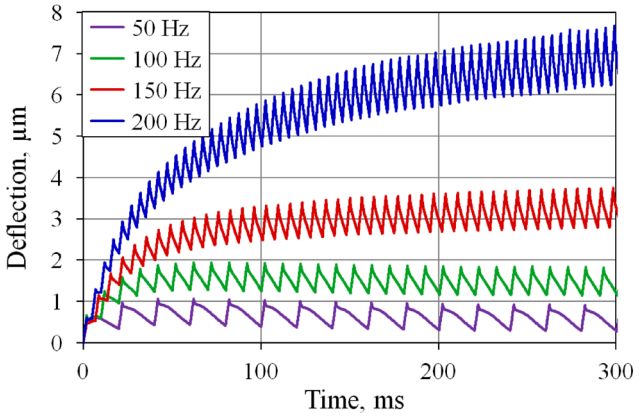


**Figure 6.** Cyclic operation of the actuator at operating frequencies of 50–200 Hz. The process is driven by a series of $N = 2000$ pulses with $f = 500$ kHz and $U = 16$ V.

can see that even with such a small stroke the relaxation time of the membrane is about 50 ms.

During the active time the deflection grows linearly with time. Then it is reduced slightly and grows again reaching a maximum at $t \approx 7$ ms. It can be explained by competition of two processes: growth and termination of nanobubbles. The concentration of nanobubbles located near the electrodes is the highest and these bubbles are terminated first. At the same time, due to high supersaturation the gases dissolved in the electrolyte continue entering the existing nanobubbles resulting in the rise of the pressure in the chamber. Finally, the termination of gases prevails, when the concentration of dissolved gases is close to the saturated one.

Cyclic operation of the actuator driven by a series with $t_a = 2$ ms is shown in figure 6. When the passive time is $t_p = 18$ ms, the device operates at $f_c = 50$ Hz. In order to obtain the frequency of 100, 150 and 200 Hz, $t_p$ is reduced to 8.0, 4.7 and 3.0 ms, respectively. The smaller $t_p$, the higher is the offset in the membrane deflection during the first few cycles. At $f_c = 200$ Hz it stabilizes at about 6.5 $\mu$m. Increase of the operating frequency leads to a longer stabilization time. At $f_c = 50$ Hz the actuator reaches the stable regime in 40 ms (two cycles), while at $f_c = 200$ Hz the stabilization takes more than 300 ms.

At $f_c = 50$ Hz the stroke is $d_{max} = 0.6$ $\mu$m, which corresponds to the maximum deflection for a single series. At this frequency $d_{max}$ is stabilized nearly from the very beginning, but at higher $f_c$ the stroke increases during the stabilization time. At $f_c = 200$ Hz it grows from 0.6 to 1.5 $\mu$m. It has to be stressed that the higher the operating frequency, the larger is the stroke in the stable regime. A combined increase of $f_c$ and $d_{max}$ gives a significant increment of the effective flow rate. At $f_c = 50$ Hz the pump would have $R = 0.19$ $\mu$l min$^{-1}$, while for $f_c = 200$ Hz the flow rate would be $R = 1.81$ $\mu$l min$^{-1}$. The dependence of $R$ on $f_c$ is non-linear, since the two factors make a contribution (see figure 7). We relate the long-time saturation of the membrane deflection with the balance between generation and termination of the gases. The faster the voltage is switched between on and off positions, the higher saturated concentration of nanobubbles can be reached

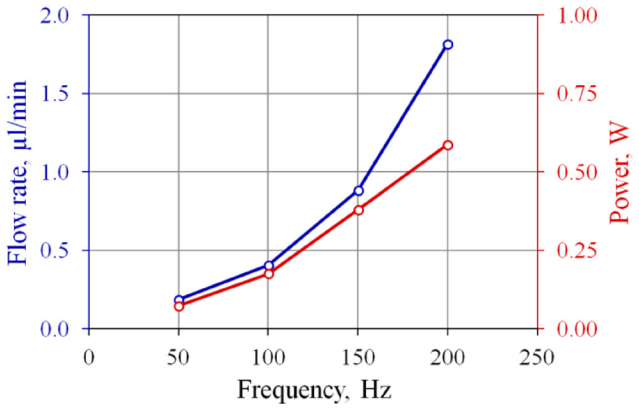


**Figure 7.** The dependence of the calculated flow rate and the power consumption of the actuator on the operating frequency.

in the chamber. It explains why the amplitude of the membrane oscillations increases with $f_c$. This phenomenon can be observed at lower amplitude of pulses, but the passive time has to be reduced in order to reach a high concentration of nanobubbles. For $U = 13$ V that has been used in the low-frequency experiment, $t_p < 1$ ms is needed, which is below the limit of the signal generator.

It is worth noting that the operating frequency of 200 kHz is not the limit. Cyclic operation at $f_c$ as high as 667 Hz with the stroke of 2 $\mu$m was demonstrated previously [33]. However, it was necessary to increase the amplitude of pulses up to $U = 22$ V due to a short active time of $t_a = 0.5$ ms. Such a high-voltage operation is not analyzed in this work.

An important characteristic of the actuators is the power consumption $P$. It is calculated from the waveforms of the voltage $U(t)$ and the current $I(t)$ flowing through the electrodes:

$$P = f_c \int_0^{t_a} U(t)I(t)dt. \quad (1)$$

The power consumption increases with the operating frequency, as one can see in figure 7. The actuator consumes 73 mW at $f_c = 50$ Hz, while at $f_c = 200$ Hz this value is $P = 587$ mW. Unlike the effective flow rate, $P$ grows almost linearly with $f_c$.

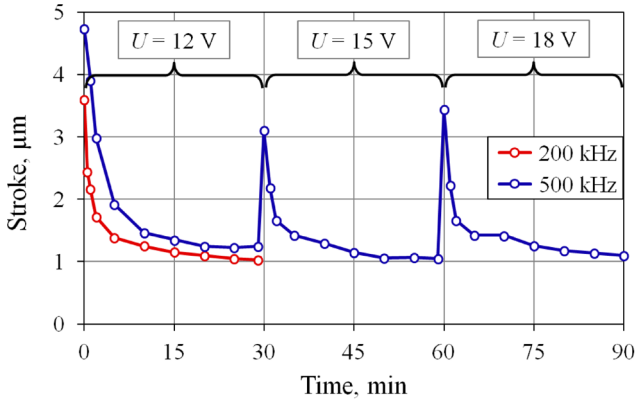


**Figure 8.** Time dependence of the stroke during the cyclic operation at $f_c = 10$ Hz. The blue line corresponds to the actuator driven by a series of $N = 20\,000$ pulses with $f = 500$ kHz. The amplitude of pulses is $U = 12$ V during the first 30 min. Then it increases to 15 V and to 18 V. The red line corresponds to another sample driven by a series of $N = 8000$ pulses with $f = 200$ kHz.

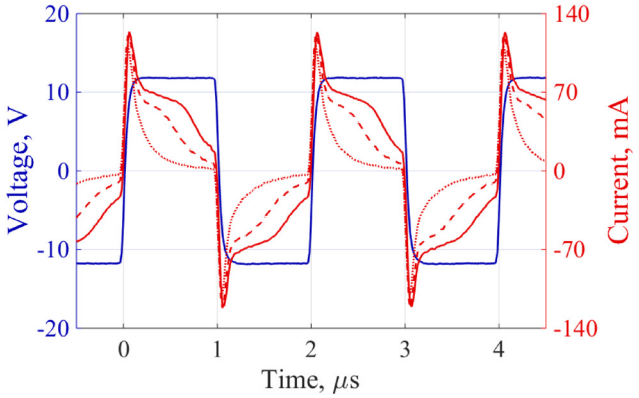


**Figure 9.** The driving voltage and the current flowing through the electrodes during the active time. The frequency of voltage pulses is $f = 500$ kHz and the amplitude is $U = 12$ V. The solid red line corresponds to the current captured at the first minute of the long-term test. The dashed and dotted lines show the current at the 3rd and 30th minutes, respectively.

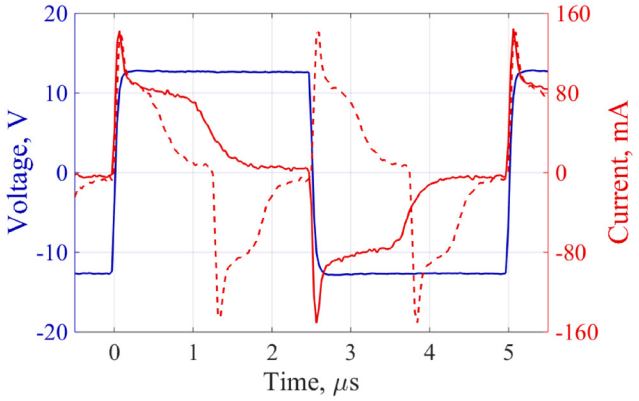


**Figure 10.** The driving voltage and the current flowing through the electrodes at various $f$. The amplitude of voltage pulses is $U = 13$ V. The voltage is shown for $f = 200$ kHz only. The solid and dashed red lines correspond to the current at $f = 200$ and 400 kHz, respectively.

However, it is reasonable to characterize actuators by the power consumed per unit flow rate that has a meaning of the energy needed to pump over a unit volume. This power goes down as the frequency increases. At $f_c = 50$–$100$ Hz this value is 433 mW $(\mu\text{l min}^{-1})^{-1}$, while at $f_c = 200$ Hz it is 324 mW $(\mu\text{l min}^{-1})^{-1}$. When the operating frequency is low (10–25 Hz), the actuator consumes 400–500 mW per 1 $\mu$l min$^{-1}$. Thus, higher operating frequency is more beneficial.

The power consumption of the actuator $P \sim 100$ mW is quite high. There are two main reasons for such a high consumption. First, not all the produced gas performs the mechanical work. The AP electrolysis generates not only $H_2$ and $O_2$ nanobubbles, but also a large number of bubbles containing mixtures of $H_2$ and $O_2$ [29]. The latter bubbles disappear very fast in the reverse reaction, which is ignited in nanobubbles spontaneously. These nanobubbles do not contribute to the mechanical work. According to the estimates less than 10% of the generated gas molecules are responsible for the pressure rise in the chamber [29]. The second reason is the oxidation of titanium electrodes during operation, which is responsible for high applied voltage. Degradation of the electrodes related to their oxidation is discussed in the following section.

### 3.4. Long-term operation

Durability of the cyclic operation is investigated at $f_c = 10$ Hz. The process is driven by a series of $N = 20\,000$ pulses with $f = 500$ kHz and $U = 12$ V. The active and passive times are 20 and 80 ms, respectively. The device works in this regime for 30 min. Figure 8 shows how the stroke changes with time. At the beginning of the test the membrane deflects at 4.7 $\mu$m, and by the 30th minute $d_{max}$ decreases to 1.0 $\mu$m. The most dramatic drop occurs in the first five minutes of operation. The stroke can be partially restored by making the amplitude of pulses higher. Increasing $U$ to 15 V at the 31st minute of the process enlarges $d_{max}$ to 3.1 $\mu$m. However, it drops again to 1.0 $\mu$m during the next 30 min. Increasing the amplitude of pulses to 18 V at the 61st minute of the test raises the stroke to 3.5 $\mu$m, but not for long. The same behavior of the stroke is observed for all frequencies of the driving pulses, but for the smaller $f$ it drops more rapidly during the first minutes of operation, see figure 8.

The stroke is determined by the amount of the gas generated during the active time. This amount is governed by the Faraday current flowing through the electrochemical cell [29]:

$$M = \frac{3}{4e}\int_0^{t_a} I_F(t)dt, \qquad (2)$$

where $M$ is the number of produced gas molecules, $e$ is the absolute value of the electron charge and $I_F(t)$ is the Faraday current. If the electrode material is not modified chemically in the electrolysis, the current flowing through the cell consists of two components [34]. The first one is the Faraday current that is constant during a microsecond voltage pulse. The second component corresponds to the charging–discharging of the double layer on the electrode surface and is not related to the electrochemical reaction. The total current is well fitted by the following time dependence [34]:

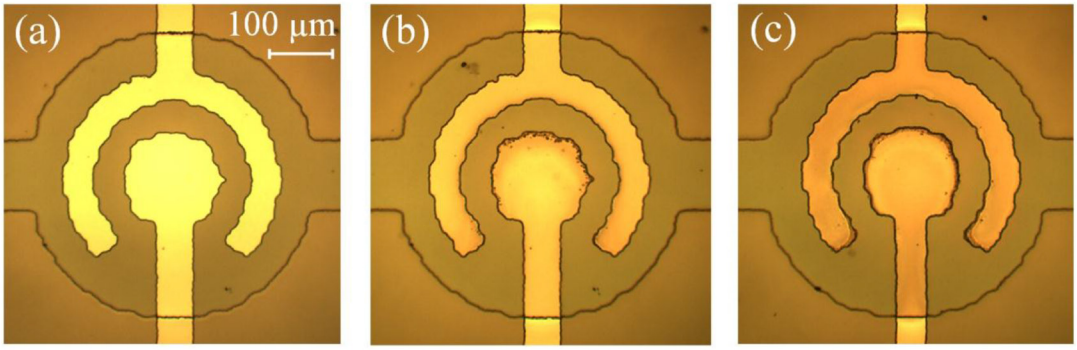


**Figure 11.** Optical image of the working chamber: (a) the fresh sample; (b, c) the samples tested at $f_c = 10$ Hz during 60 min. The samples (b) and (c) were driven by the pulses with $f = 500$ and 200 kHz, respectively. In both cases $U = 12$ V and $t_a = 20$ ms.

$$I(t) = I_F + I_1 e^{-t/\tau}, \tag{3}$$

where $I_1$ is a constant and $\tau$ is the relaxation time related to the capacitance of the double layer.

However, in our case $I_F$ cannot be extracted using this approach due to a peculiar shape of the current pulse. Two periods of the driving voltage and the current are shown in figure 9. At the beginning of the test, the current pulse has a peak and a flat region that is followed by a fall. The peak corresponds to the charging–discharging of the double layer, but the Faraday current is not constant during the voltage pulse. To all appearance, an additional component, which is responsible for the oxidation-reduction of titanium electrodes, contributes to the current. The pulse changes the shape with time. The high-current plateau moves down and shortens, while the low-current plateau emerges (see the waveform captured at the 3rd minute). Finally, the characteristic hump disappears. Only the peak and the low-current plateau are visible at the 30th minute of operation. In order to compare the currents at different moments, we use the average current $I_{AV}$ flowing through the electrodes. The waveform is integrated over $t_a$, and the obtained value is divided by this time interval. For the negative pulses we take the absolute values of the current. The evolution of the shape results in the drop of $I_{AV}$ and in the reduced gas production. In the 1st minute the average current is $I_{AV} = 69$ mA, while for the 30th minute we obtain $I_{AV} = 24$ mA. In the AP electrolysis, an oxide layer is formed on the electrode over half of the period, but then it is reduced over the second half. To all appearance, the oxidation process dominates the reduction since the average current drops.

Analysis of the waveforms also reveals why the higher frequency of pulses provides the higher stroke. For the test described in Section 3.1 the current pulse has a peak, a flat region that is followed by the fall, and a flat region with a low current (see figure 10). The peak has the same size for all $f$. The flat regions shorten as the frequency increases, but the low-current region shrinks stronger. It is almost absent at the waveform corresponding to $f = 400$ kHz. As a result, the average current increases with $f$ that correlates with the increase of the stroke. For $f = 100$ kHz the calculation gives $I_{AV} = 29$ mA, while for $f = 500$ kHz we obtain $I_{AV} = 42$ mA.

The oxidation manifests itself as a darkening of the electrodes, see figure 11. It is known from the DC electrolysis that an oxide film formed on the titanium anode changes the color due to light interference [35]. At the initial stage of growth the film is yellow, and then it turns brown as the thickness increases [35, 36]. In the AP process, each electrode periodically plays the role of anode and, therefore, undergoes the oxidation and changes the color. The edge of the inner electrode and the corners of the outer electrode are darker than the other parts due to the higher current density in these places. The darkening is observed at all frequencies of pulses, but for lower $f$ it is more pronounced. To all appearance, for low frequencies the electrodes are oxidized faster. It is worth noting that except of oxidation no other sign of degradation is observed in the non-explosive regime.

The oxidation increases the power consumption of the actuator, since one has to increase the amplitude of pulses in order to maintain the stroke at the sufficient level. At the 3rd minute of the test the membrane deflects at 3.0 $\mu$m (figure 8). The amplitude of pulses is $U = 12$ V, and the device consumes $P = 104$ mW. At the 31st minute the stroke has a close value of 3.1 $\mu$m, but at the higher amplitude of $U = 15$ V. In this regime $P = 191$ mW. At the 61st minute $d_{max} = 3.4$ $\mu$m at $U = 18$ V. The power consumption increases to 227 mW. Therefore, the problem of electrode degradation is crucial for the actuator based on the AP electrolysis. It is desirable to use a material that is not oxidized during operation. Noble metals such as gold or platinum do not undergo oxidation, but they cannot withstand a high current density of the AP process [34, 37]. Titanium demonstrates the best durability, but the oxidation problem has to be overcome. One possible way is to choose the deposition conditions of Ti that suppress the oxidation. Another way is to select the operation regime, in which the oxidation process is compensated by the reduction. This can be done by increasing the amplitude of the reduction voltage pulse. For the actuator with two electrodes this method will not work, because stronger reduction of one electrode leads to stronger oxidation of another electrode. Nevertheless, this idea can be realized in the three-electrode system, where one electrode is grounded and the other electrodes can be oxidized and reduced independently. We plan to implement these techniques in order to enhance the performance of the actuator.

## 4. Conclusion

Operation of the fast electrochemical actuator in the non-explosive regime was investigated in detail. The device was driven by a series of AP voltage pulses. The frequency of the pulses was varied from 100 to 500 kHz. A higher frequency provides a larger membrane deflection. In addition, it allows operation at higher amplitude of the pulses without explosions. Therefore, even larger stroke can be achieved. When the pulses are switched off, the membrane returns to its initial state in 40–60 ms. This relaxation time is determined by the gas recombination rate and the elastic properties of the membrane. When the time interval between the series exceeds the relaxation time, the membrane returns to its initial position at each cycle, but the operating frequency of the device is limited by 10–20 Hz. If the passive time is shorter than the relaxation time, the gas is collected in the chamber and the membrane oscillates in the lifted position. The magnitude of the lift reaches 6–7 $\mu$m. A high concentration of nanobubbles is always maintained in the chamber, providing a faster recombination of the gas. The stroke of the membrane increases with the operating frequency, which makes the higher frequency more beneficial in terms of power consumption. However, the actuator consumes a fairly high power ~100 mW. One of the reasons is the oxidation of titanium electrodes, which reduces the current flowing through the electrolyte and the amount of the gas produced during the active time. The stroke decreases in the long-term operation, and one has to increase the driving voltage in order to maintain it. At a high frequency of the pulses the oxidation goes slower, but still significantly affects the performance of the actuator. Nevertheless, titanium electrodes demonstrate no signs of destruction in the non-explosive regime.

## Acknowledgments

This work is supported by the Russian Science Foundation, Grant No. 18-79-10038.

## ORCID iDs

Ilia V Uvarov https://orcid.org/0000-0002-6882-0625
Vitaly B Svetovoy https://orcid.org/0000-0002-9649-5663

## References

[1] Sackmann E K, Fulton A L and Beebe D J 2014 *Nature* **507** 181
[2] Yeo L Y, Chang H-C, Chan P P Y and Friend J R 2011 *Small* **7** 12
[3] Temiz Y, Lovchik R D, Kaigala G V and Delamarche E 2015 *Microelectron. Eng.* **132** 156
[4] Mark D, Haeberle S, Roth G, von Stetten F and Zengerle R 2010 *Chem. Soc. Rev.* **39** 1153
[5] Cobo A, Sheybani R and Meng E 2015 *Adv. Healthc. Mater.* **4** 969
[6] Riahi R, Tamayol A, Shaegh S A M, Ghaemmaghami A M, Dokmeci M R and Khademshosseini A 2015 *Curr. Opin. Chem. Eng.* **7** 101
[7] Amirouche F, Zhou Y and Johnson T 2009 *Microsyst. Technol.* **15** 647
[8] Zhao B, Cui X, Ren W, Xu F, Liu M and Ye Z-G 2017 *Sci. Rep.* **7** 11319
[9] Dumont-Fillon D, Tahriou H, Conan C and Chappel E 2014 *Micromachines* **5** 1161
[10] Machauf A, Nemirovsky Y and Dinnar U 2005 *J. Micromech. Microeng.* **15** 2309
[11] Zengerle R, Ulrich J, Kluge S, Richter M and Richter A 1995 *Sensors Actuators* A **50** 81
[12] Yamahata C, Lotto C, Al-Assaf E and Gijs M A M 2005 *Microfluid. Nanofluid.* **1** 197
[13] Spieth S, Schumacher A, Holtzman T, Rich P D, Theobald D E, Dalley J W, Nouna R, Messner S and Zengerle R 2012 *Biomed Microdevices* **14** 799
[14] Ha S-M, Cho W and Ahn Y 2009 *Microelectron. Eng.* **86** 1337
[15] Li P-Y, Sheybani R, Gutierrez C A, Kuo J T W and Meng E 2010 *J. Microelectromech. Syst.* **19** 215
[16] Sheybani R, Cobo A and Meng E 2015 *Biomed. Microdevices* **17** 74
[17] Sheybani R, Gensler H and Meng E 2013 *Biomed. Microdevices* **15** 37
[18] Sheybani R and Meng E 2012 *J. Microelectromech. Syst.* **21** 1197
[19] Yi Y, Buttner U, Carreno A A A, Conchouso D and Foulds I G 2015 *J. Micromech. Microeng.* **25** 105011
[20] Yi Y, Buttner U and Foulds I G 2015 *Lab Chip* **15** 3540
[21] Sheybani R and Meng E 2015 *Sensors Actuators* B **221** 914
[22] Lee D E, Soper S and Wang W 2008 *Microsyst. Technol.* **14** 1751
[23] Lee D E, Soper S and Wang W 2006 *Proc. SPIE* **6112** 61120N
[24] Lui C, Stelick S, Cady N and Batt C 2010 *Lab Chip* **10** 74
[25] Xie J, Miao Y, Shih J, He Q, Liu J, Tai Y-C and Lee T D 2004 *Anal. Chem.* **76** 3756
[26] Kim H, Hwang H, Baek S and Kim D 2018 *Sensors Actuators* A **277** 73
[27] Postnikov A V, Uvarov I V, Penkov N V and Svetovoy V B 2018 *Nanoscale* **10** 428
[28] Svetovoy V B, Sanders R G P, Lammerink T S J and Elwenspoek M C 2011 *Phys. Rev.* E **84** 035302
[29] Svetovoy V, Postnikov A, Uvarov I, Sanders R and Krijnen G 2016 *Energies* **9** 94
[30] Prokaznikov A, Tas N and Svetovoy V 2017 *Energies* **10** 178
[31] Jain S and Qiao L 2018 *J. Phys. Chem.* A **122** 5261
[32] Uvarov I V, Postnikov A V, Shlepakov P S, Naumov V V, Koroleva O M, Izyumov M O and Svetovoy V B 2017 *J. Phys.: Conf. Ser.* **917** 082006
[33] Uvarov I V, Lokhanin M V, Postnikov A V, Melenev A E and Svetovoy V B 2018 *Sensors Actuators* B **260** 12
[34] Svetovoy V B, Sanders R G P and Elwenspoek M C 2013 *J. Phys.: Condens. Matter* **25** 184002
[35] Van Gils S, Mast P, Stijns E and Terryn H 2004 *Surf. Coat. Technol.* **185** 303
[36] Delplancke J-L, Degrez M, Fontana A and Winand R 1982 *Surf. Technol.* **16** 153
[37] Uvarov I V, Melekhov S S, Melenev A E and Svetovoy V B 2016 *J. Phys.: Conf. Ser.* **757** 012008